LAWRENCE
LIVERMORE
NATIONAL
LABORATORY

UCRL-TR-226799

Determination of Optimum Conditions for Distinguishing the Pulse Height Distributions of Atomic and Polyatomic Ions

M. J. Kristo

December 13, 2006

This work was performed under the auspices of the U.S. Department of Energy by University of California, Lawrence Livermore National Laboratory under Contract W-7405-Eng-48.

UCRL-TR-226799

Determination of Optimum Conditions for Distinguishing the Pulse Height Distributions of Atomic and Polyatomic Ions

Work Performed in Years 1 and 2

For Project #LL318DP, Task 1

Deliverables D1/FY05 & D1/FY06

December 14, 2006

By
Lawrence Livermore National Laboratory

M. J. Kristo

Under Contract to:
DOE/NA22

Deliverable D1/FY05 & D1/FY06 for LL318DP

Determination of Optimum Conditions for Distinguishing Between the Pulse Height Distributions of Atomic and Polyatomic Ions

Table of Contents

Executive Summary

This work explored the use of pulse height distributions (PHD) from multiplier-type detectors as a means of detecting and eliminating the effects of polyatomic interferences in secondary ion mass spectrometry (SIMS). We explored the behavior of PHD for $^{235}U^{+}$, $^{208}Pb^{27}Al^{+}$ and $^{207}Pb^{28}Si^{+}$, all with a nominal mass-to-charge ratio of 235. In every case, the distribution for the atomic ion ($^{235}U^{+}$) was clearly shifted relative to the distributions for $^{208}Pb^{27}Al^{+}$ and $^{207}Pb^{28}Si^{+}$. When the first surface of the detector is metallic in character, the polyatomic ions are shifted to larger pulse heights relative to the atomic ion. When the first surface of the detector is oxide in character, the atomic ion is shifted to larger pulse heights relative to the polyatomic ions. The relative positioning appear to be stable for a given detector over time at the same secondary ion impact energy. Consequently, it appears to be feasible to use PHD data to detect interfering polyatomic ions and eliminate their deleterious effects using peak deconvolution techniques. Consequently, the updated Ultrafast RAE detector will be designed to make the pulse height information available to the data acquisition system.

Task Description

Ion detectors used in secondary ion mass spectrometry (SIMS) include multiplier-type detectors like the ETP Model AF133H and resistive anode encoders (RAE) like those sold by Quantar Technology. The distributions of pulse heights from these detectors are measurably different for atomic secondary ions, such as $^{235}U^{+}$, and polyatomic ions of the same mass, e.g., $^{208}Pb^{27}Al^{+}$ or $^{207}Pb^{28}Si^{+}$. The pulse height distributions overlap to some extent, but may be amenable to deconvolution using conventional peak-stripping techniques. We have sought to develop new, automated techniques based on pulse height analysis in order to detect and discriminate against secondary ion signals from polyatomic species that interfere with the measurement of uranium isotopic data. We specifically proposed to determine the optimum experimental conditions for separating the atomic and polyatomic distributions, e.g., by using techniques such as post-acceleration.

If complete separation proved possible, then the polyatomic ions could be rejected in hardware through the implementation of a minimum or maximum pulse height criterion. If complete separation proved impossible, then, by modifying the RAE electronics to provide pulse height information in real time, in addition to the spatial coordinate information currently provided, we could use software techniques to detect these interferences and eliminate their deleterious effects on isotopic ratios. The detector pulse height is already, in fact, used in the current RAE detector electronics to calculate the ion's x and y position. However, the pulse height is not available outside the RAE detector electronics, e.g., to the data acquisition system. With the pulse height and spatial information for each ion, the particle search software can reconstruct a pulse height distribution for any defined area, including particles identified in the particle recognition software. Consequently, the software might be able to detect the presence of polyatomic interferences in the acquired data and, through the use of standard peak-stripping techniques, correct the resulting isotope ratios for the contributions from polyatomic ions. This improvement would enable the elimination of any interfering signals and the calculation of the correct isotopic ratio for uranium.

<u>The successful completion of this project would be an improvement in the accuracy of isotope ratios determined by SIMS.</u>

Theory

The difference between the pulse height distributions for atomic and polyatomic ions has been known for some time.[1-2] Additional research conducted in the late 1970's and early 1980's improved the understanding of ion-electron emission as part of efforts to design better ion detectors. Differences in pulse height distributions from an electron multiplier or RAE detector is primarily determined by the distribution of secondary ions released by ion impact at the first surface of the detector (the conversion dynode). The subsequent amplification of the resulting electron signal by electron-electron emission at subsequent dynodes adds variance to the

[1] H. E. Stanton, W. A. Chupka, and M. A. Inghram, *Rev. Sci. Instrum.* **27**, 109 (1956).
[2] C. LaLau, in A. L. Burlingame (Ed.), *Advances in Analytical Chemistry and Instrumentation* (Wiley Interscience, New York, 1970), Vol. 8, p. 93.

resulting pulse height distribution, but does not, in general, vary systematically based upon the nature of the impacting ion.

The relationship between the pulse height distributions (PHD) for atomic and polyatomic ions is explained by several related observations. The first observation is that the average number of electrons released by an ion at the first surface of the detector (designated as γ or N_p) increases with increasing ion atomic number (Z) at constant ion velocity, but that the slope of the γ-vs-Z curve decreases with increasing Z.[3,4,5,6] The second observation is that, for many metal surfaces, γ for polyatomic ions is equal to the sum of the γ's for each of the constituent atoms.[7,8,9] Note that the constituent atoms have the same impact velocity as the parent polyatomic ion. This implies that, for metal surfaces, γ for polyatomic ions will always be greater than γ for atomic ions of the same mass.

The third observation is that, for Al_2O_3 surfaces, γ for polyatomic ions is less than the sum of the γ's for each of the constituent atoms at the same impact velocity.[10] The different behavior for Al_2O_3 (and possibly other non-conducting surfaces) has not been thoroughly explained, but may be related to the build-up of charge on the surface of the detector during the emission process, leading to a suppression of further electron emission. This, in turn, suggests that, for Al_2O_3 surfaces, γ for polyatomic ions may be less than γ for atomic ions of the same mass. Because of the decreasing slope of the γ-vs-Z curve, this shift to a lower PHD than to the corresponding atomic ion would be particularly pronounced for polyatomic ions of large mass containing a large constituent atom, e.g., $^{208}Pb^{27}Al^+$ or $^{207}Pb^{28}Si^+$. In any event, we must expect different behavior between ion detectors with metal surfaces and detectors with oxide surfaces.

Experimental

Secondary Ion Mass Spectrometry

In order to explore the "polyatomic vs. atomic" effect for ^{235}U and the above-mentioned lead-based interferences, we used our CAMECA 3f instrument to acquire pulse height distributions for positive secondary ions with a mass-to-charge ratio of 235 using U_3O_8 particles (NBL U900) to generate $^{235}U^+$, an improvised sample of lead particles on aluminum to generate $^{208}Pb^{27}Al^+$, and an improvised sample of lead particles on a silicon wafer to generate $^{207}Pb^{28}Si^+$. These samples were analyzed using an O_2^+ primary ion beam with an impact energy of 5.5 keV (10.0 kV accelerating potential with the sample potential at 4.5 kV). For ion detection, we used both an electron multiplier (ETP Model AF133H) and a fast resistive anode encoder (Quantar Technology, Model 3390A).

---

[3] C. Lao, R. Sander, and R. F. Pottie, *Int. J. Mass Spectrom. Ion Phys.*, 10 (1972/73) 309.
[4] U. Fehn, *Int. J. Mass Spectrom. Ion. Phys*., 21 (1976) 1.
[5] R. J. Beuhler and L. Friedman, *Int. J. Mass Spectrom. Ion Phys*., 23 (1977) 81.
[6] L. A. Dietz and J. C. Sheffield, *J. Appl. Physics* 46 (1975) 4361.
[7] F. Thum and W. O. Hofer, *Surface Science* 90 (1979) 331.
[8] R. J. Beuhler and L. Friedman, *Nucl. Instrum. Methods* 170 (1980) 309.
[9] Beuhler and Frieman, *Int. J. Mass Spectrom. Ion Phys*., 10 (1977) 81.
[10] R. J. Beuhler, *J. Appl. Physics*, 54 (1983), 4118.

In order to explore the effect of ion impact energy on the polyatomic effect, I conducted a series of experiments using a CAMECA ims-4f with the CAMECA post-acceleration option[11] located at the National Institute of Standards & Technology (NIST) in Gaithersburg, MD. Using the same samples described above, I studied the effect of increasing and decreasing secondary ion energy on the pulse height distributions of polyatomic and atomic ions. I operated the CAMECA post-acceleration chassis in the positive ion mode. Therefore, increasing the post-acceleration voltage meant floating the electron multiplier detector and housing at an increasingly negative voltage, thus increasing the impact energy of the incoming positive ions. I also explored the effect of decreasing the ion impact energy of positive ions by switching to negative ion mode. Increasing the post-acceleration voltage in negative ion mode meant floating the detector assembly at an increasingly positive voltage, thus decreasing the impact energy of the incoming positive ions.

The normal energy for secondary ions in a CAMECA 3f or 4f is 4.5 keV when using a multiplier with a grounded entrance or 4.5 keV plus the multiplier voltage for a multiplier with a grounded anode. For the LLNL ims-3f, the electron multiplier was operated with a grounded anode, so the ion impact energy was equal to 4.5 keV plus an additional energy (nominally 2.3 keV) determined by the exact multiplier voltage. The RAE was operated with a grounded face, so that the ion impact energy was always equal to 4.5 keV.

Electronics

Both the LLNL and NIST instruments were controlled by the Charles Evans & Associates PSEARCH-PXT system.[12] We developed specialized electronics to study the pulse height distributions from either an electron multiplier or RAE detector. We used a PC-based Ortec Trump PCI-16K multichannel analyzer to quickly the acquire pulse height spectra. We used an Ortec Model 672 Spectroscopy Amplifier, followed by an Ortec Model 542 Linear Stretcher, to interface the extremely fast pulse height signals from the electron multiplier or RAE to the fairly slow multichannel analyzer (see Figure 1). Both spectroscopy amplifier and linear stretcher were NIM-based electronics.

[11] CAMECA User's Guide EM Post-Acceleration, Ref # 45 403 964.
[12] Charles Evans & Associates, Sunnyvale, CA.

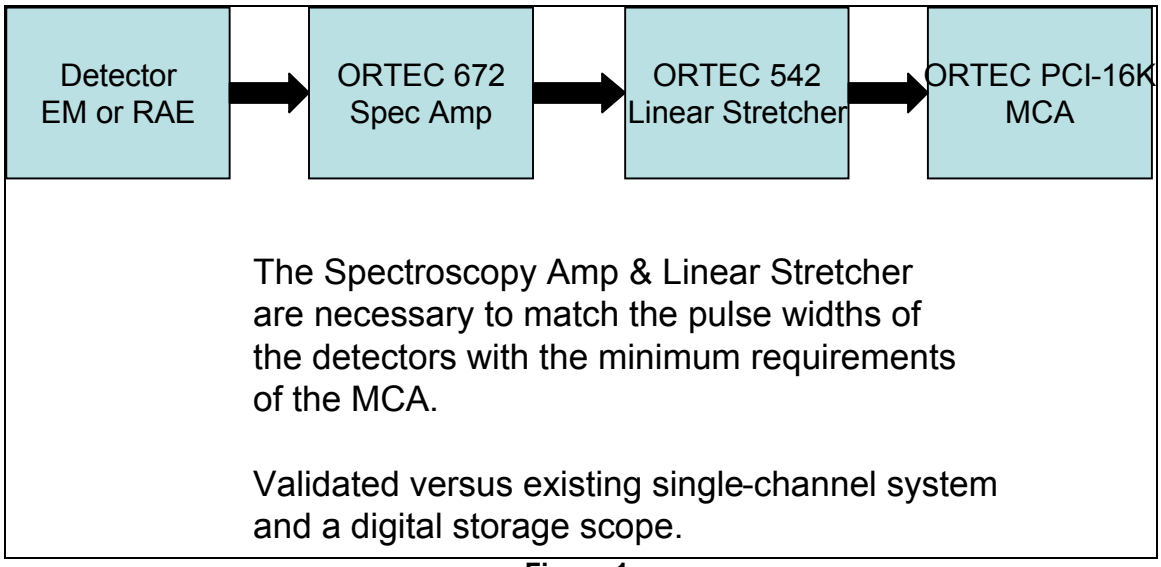

Figure 1.
Schematic Design of the Multichannel Pulse Height Analyzer System

I verified the basic performance of the system by using pulses generated by a Hewlett Packard 8082A Pulse Generator as the input into the Ortec Spectroscopy Amplifier and measuring the resulting pulse height distributions using the Ortec Maestro 32 software. The input pulses were roughly triangular shaped and approximately 20 ns in width at the base of the pulse. The pulse rate was approximately 30 kHz and was kept constant during each set of measurements. I determined the pulse heights by measuring them directly on a Tektronix TDS 5054B oscilloscope (500 MHz). The resulting pulse height distributions were very narrow, approximately Gaussian-shaped peaks. Figures 2 and 3 show plots of the centroid of the resulting PHD peak (in ADC units) versus the amplitude of the input pulse for two different gain settings. The linearity is excellent.

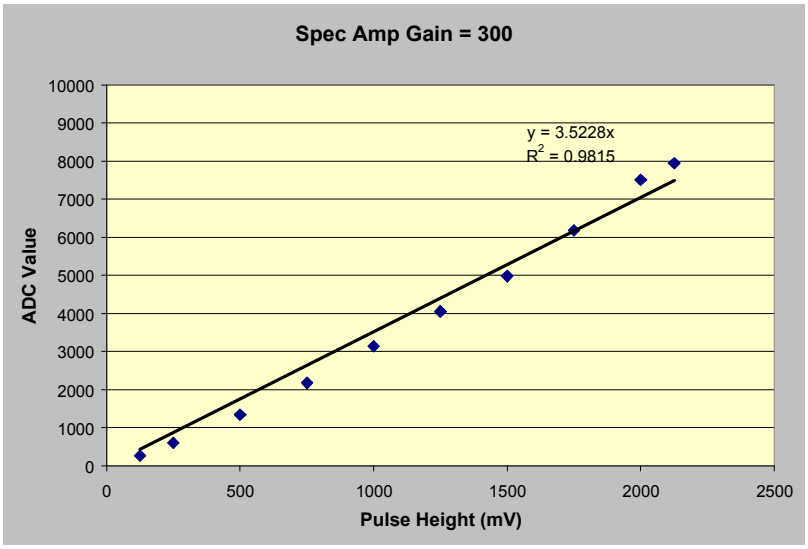

Figure 2
Gain of the entire system using a Spectroscopy Amp Gain of 300 (τ=0.5 μs)

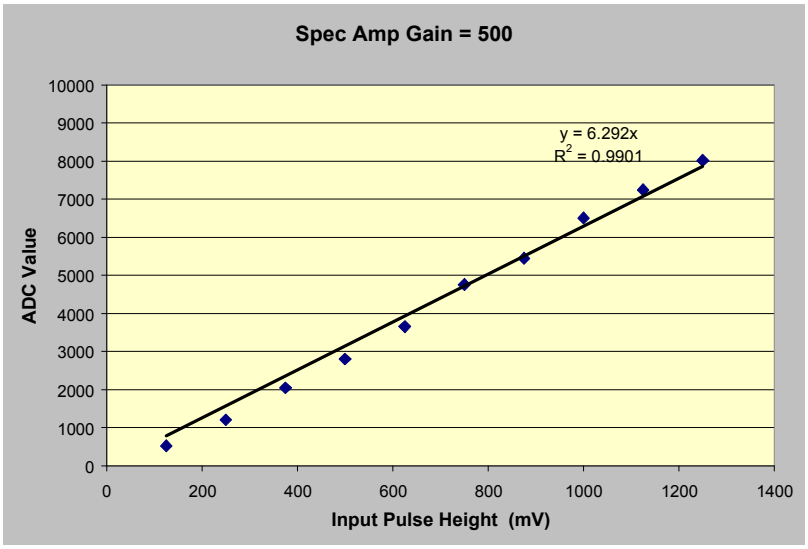

Figure 3
Gain of the entire system using a Spectroscopy Amp Gain of 500 (τ=0.5 μs)

In order to determine the reproducibility and repeatability of the pulse height distributions, I acquired 9 pulse height distributions each for $^{12}C^+$, $^{27}Al^+$, $^{28}Si^+$, $^{48}Ti^+$, $^{207}Pb^+$, $^{208}Pb^+$, $^{235}U^+$, $^{27}Al^{208}Pb^+$, and $^{28}Si^{207}Pb^+$. I measured the $^{207}Pb^+$ and $^{208}Pb^+$ distributions twice – once on the PbAl sample and once on the PbSi sample. I acquired 3 pulse height distributions in quick succession, without removing the sample holder or making any other substantive changes, for each species on 3 different days. I removed each sample holder after the set of 3 measurements, in order to introduce the next sample. Each set of 3 measurements can be considered a "best case" for estimating the precision of the measurement. The variability within the 9 measurements for each species can be considered a practical "worse case" scenario for precision over a short period of time (days to weeks).

Software Methods

I used two methods to analyze the pulse height distributions generated during these experiments. The first was the calculation of the weighted average pulse height, which I called "gamma." Gammas calculated at a constant electron multiplier voltage should be proportional to the average number of electrons per ion released at the multiplier cathode (γ or N_p), as long as the multiplier gain remains constant. This should be true as long as the multiplier voltage is kept constant and the measurements are taken over a short time period (days to weeks).

The second method of analyzing the experimental PHD was to fit each distribution to a Voigt function using the peak-fitting module in Origin Pro 7.5. Figure 4 shows Origin's mathematical description of the Voigt function. The result of the fitting process provides estimates of the Voigt "center" and full-width half maximum (FWHM). The terms "center" and "FWHM" in this report refer to the Voigt parameters that are outputs of fitting a Voigt function to the experimental PHD.

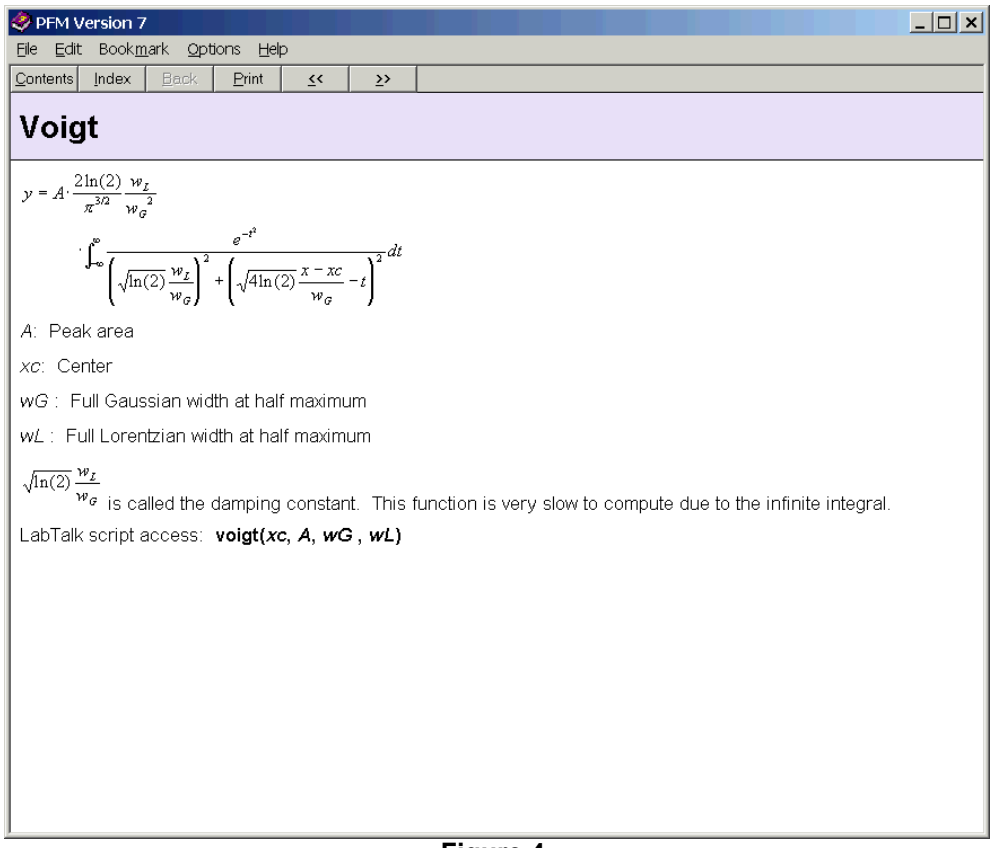

Figure 4.
Description of the Voigt Function in Origin 7.5

Distributions used by other authors in theoretical analyses of pulse height distributions include the Polya and binomial distributions,[13] as well as the Poisson distribution[14] However, because they contain factorials, none of these functions are amenable to automated curve-fitting routines. I empirically tested every curve fitting function available in Origin and selected the Voigt function as the most robust in closely matching the experimental pulse height distributions. The correlation coefficient between the fitted Voigt function and the experimental data was typically 0.97 or greater. Using either the gamma value or the peak center and FWHM generated via curve-fitting, we can examine, in a quantitative way, how the pulse height distributions (PHD) vary with species and post-accelerating voltage.

In order to describe the variability in these measurements, I will use the commonly accepted definition of repeatability as *within-run* (short-term) variability and reproducibility as *between-run* (longer-term) variability. The repeatability of the Voigt center within the sets of 3 measurements ranged from 0.04%-7.3% with an average of 1.2%. The repeatability of the Voigt FWHM ranged from 0.3%-5.1% with an average of 0.9%. The reproducibility determined from all 9 of these measurements is shown for each species in Table 1.

[13] L. A. Dietz, "Electron Multipliers and Statistics of Secondary Electron Emission," General Electric Company, Knolls Atomic Power Laboratory, KAPL-P-3879.
[14] G. Slodzian, M. Chaintreau, R. Dennebouy, and A. Rousse, Eur. Phys. J. AP, 14, 199-231 (2001).

Table 1
Reproducibility of PHD Measurements

Species	Sample	Center	Width
C12	Graphite	2.4%	2.5%
Al27	PbAl	2.9%	4.9%
Si28	PbSi	1.1%	2.9%
Ti48	Ti	6.0%	5.0%
Pb207	PbAl	4.8%	2.1%
Pb207	PbSi	2.5%	2.7%
Pb208	PbAl	6.1%	2.5%
Pb208	PbSi	1.9%	2.5%
U235	U	4.6%	2.5%
PbAl	PbAl	3.9%	2.7%
PbSi	PbSi	5.3%	3.5%

In Figure 5, we can also see that the ratio (Voigt FWHM/center) decreases as the Voigt center increases, as predicted by Slodzian (given as L/N_M in that paper).[15]

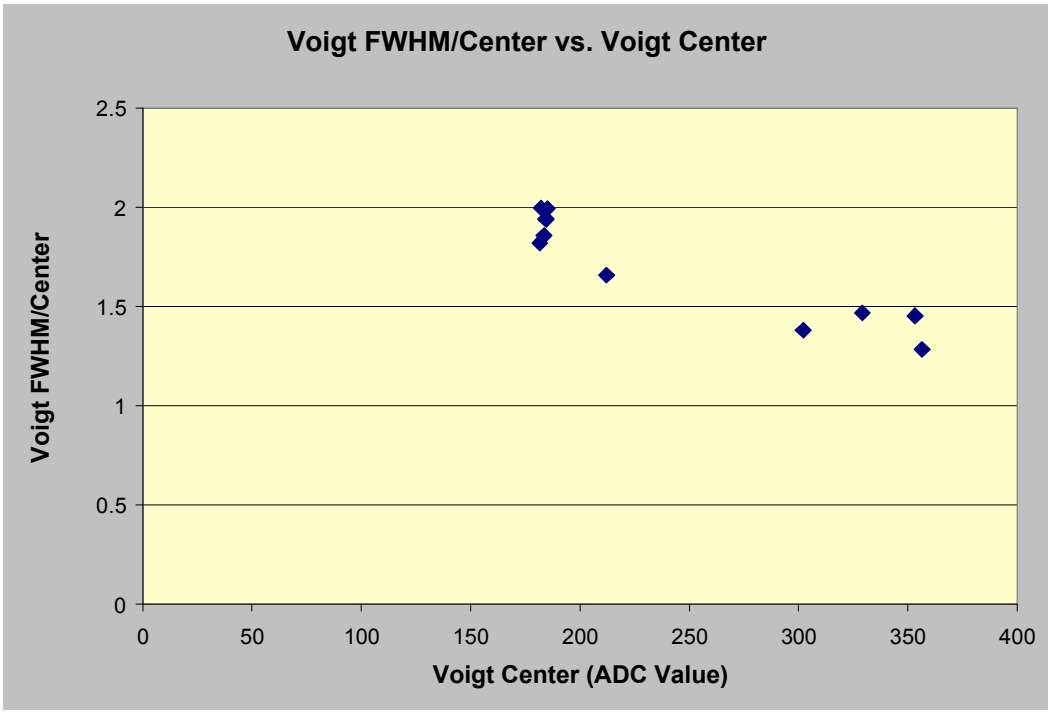

Figure 5.
Ratio (Voigt FWHM/Center) versus Voigt Center

The repeatability of the gamma measurements within the sets of 3 measurements ranged from 0.09%-5.3%, with an average of 0.9%. The reproducibility for these gamma measurements is shown for each species in Table 2.

[15] G. Slodzian, M. Chaintreau, R. Dennebouy, and A. Rousse, Eur. Phys. J. AP, 14, 199-231 (2001).

Table 2.
Repeatability of Gamma Measurements

Species	Sample	Precision
C12	Graphite	2.1%
Al27	PbAl	3.6%
Si28	PbSi	1.8%
Ti48	Ti	6.2%
Pb207	PbAl	2.6%
Pb207	PbSi	2.3%
Pb208	PbAl	3.4%
Pb208	PbSi	1.9%
PbAl	PbAl	2.7%
PbSi	PbSi	3.6%
U235	U	3.9%

Figure 6 shows that the gamma values decrease with increasing mass-to-charge ratio in a manner similar to that described by Pottie et al.[16] and Udo Fehn.[17] Note that these data are for constant ion energy, not constant ion velocity, as discussed in the Theory section.

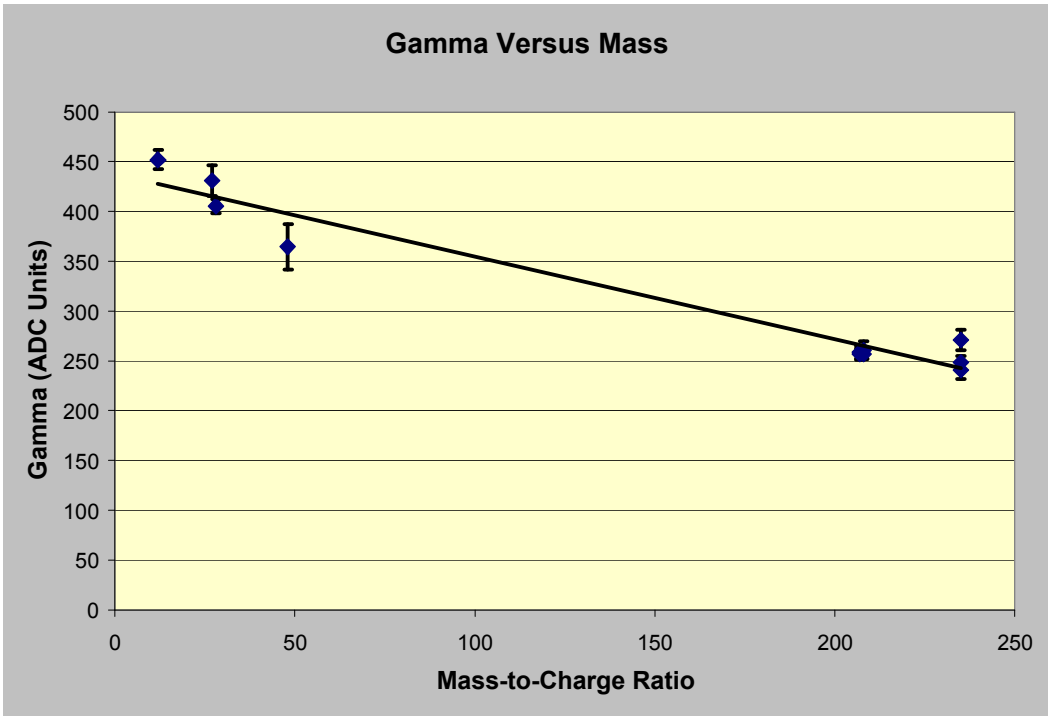

Figure 6.
Gamma vs. Mass

I compared the relative gamma values obtained in this project with those reported in the literature. Unfortunately, because different authors studied different sets of ions using different surfaces and different impact energies, direct comparison is not possible. In general, though, our gamma values (relative to ^{28}Si) are within 15% of reported literature results for most

[16] R. F. Pottie, D. L. Cocke, and K. A. Gingerich, *Int. J. Mass Spectrom. Ion. Phys*., 11 (1973) 41.
[17] U. Fehn, *Int. J. Mass Spectrom. Ion. Phys*., 15 (1974) 391.

elements. [18-19] The relative gamma value for ^{208}Pb determined in this work, however, is twice as large as that reported by other authors. We used a different surface than the other authors, who used CuBe and Al surfaces, which may account for the difference in results. No other author has reported a relative secondary electron coefficient for U.

Figure 7 shows the gamma values versus secondary ion species. Interestingly, there is very little difference between the gamma values for ^{207}Pb, ^{208}Pb, ^{235}U, $^{208}Pb^{27}Al$, and $^{207}Pb^{28}Si$. Again, these data are for constant ion impact energy, not constant ion impact velocity, as described earlier.

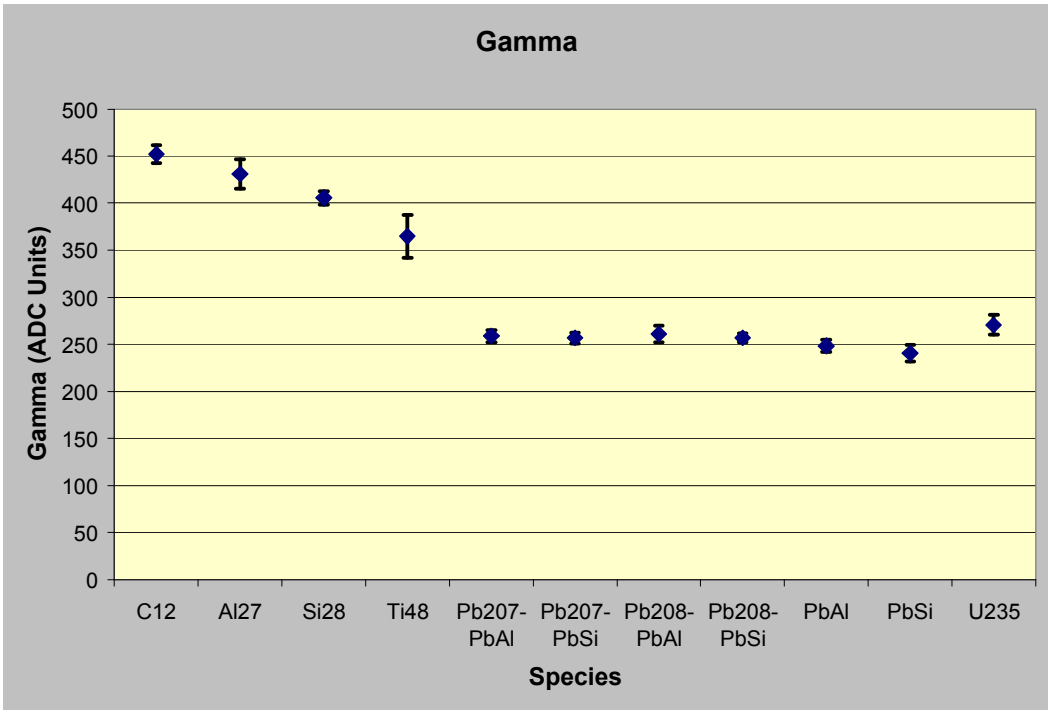

Figure 7.
Gamma vs. Secondary Ion Species

Results

Pulse Height Distributions at M/Z 235

Our initial measurements (see Figure 8) showed that the PHD for $^{235}U^{+}$ was shifted towards lower pulse heights than those for either the $^{207}Pb^{28}Si^{+}$ or $^{208}Pb^{27}Al^{+}$ interferences by about 25% (60 mV), as the theory for metal surfaces predicted. This difference proved reproducible in these initial experiments. However, subsequent measurements on 2 other ion multipliers (see Figure 9) produced PHD for $^{235}U^{+}$ that were shifted towards larger pulse heights than the PHD for either the $^{207}Pb^{28}Si^{+}$ or $^{208}Pb^{27}Al^{+}$ interferences, which is opposite to the behavior predicted by the theory for metal surfaces. Another worker in this laboratory acquired PHD for

[18] U. Fehn, Ibid.
[19] U. Fehn, Int. *J. Mass Spectrom. Ion. Phys.*, 21 (1976) 1.

$^{56}Fe^{+}$ and $^{28}Si_2^{+}$ during this period and found that the PHD for $^{28}Si_2^{+}$ was shifted clearly to larger pulse heights compared to $^{56}Fe^{+}$ in accord with the theory for metals. Clearly, the nature of the $^{207}Pb^{28}Si^{+}$ or $^{208}Pb^{27}Al^{+}$ ions played a role in this discrepancy – either due their larger mass or the large fraction of mass taken up by the Pb atom.

The fast RAE (see Figure 10) also produced PHD for $^{235}U^{+}$ that were shifted towards larger pulse heights than the PHD for the $^{207}Pb^{28}Si^{+}$ or $^{208}Pb^{27}Al^{+}$interferences. The results from the fast RAE confirmed, though, that PHD from RAE detectors show the same effects as those from ion multipliers, which have been much more widely studied in the literature.

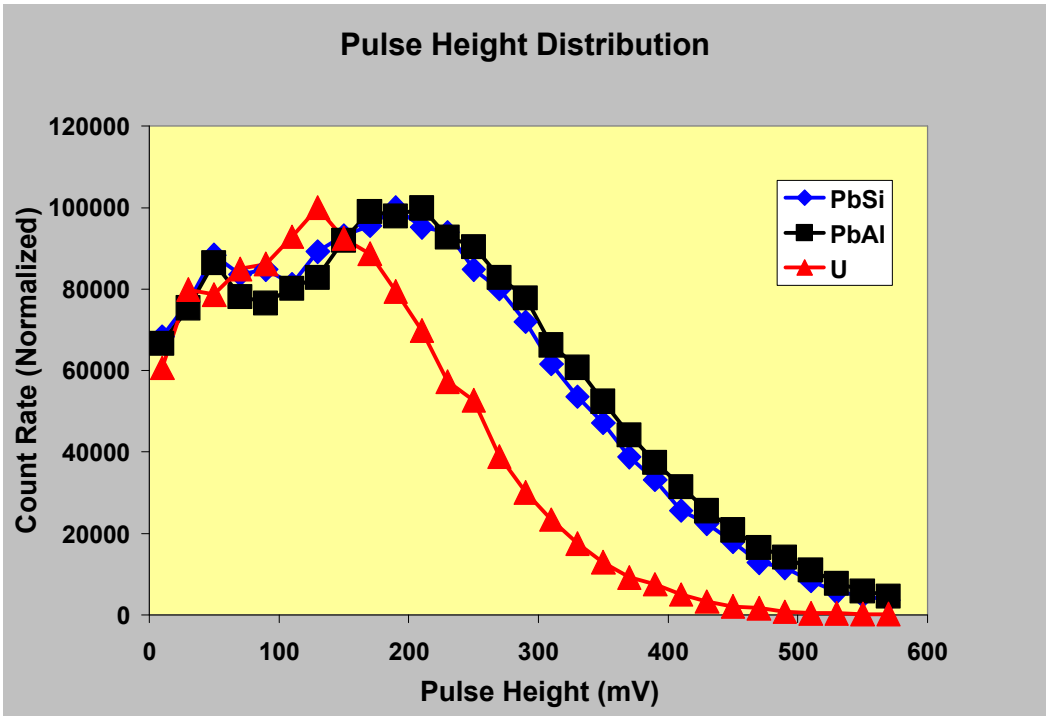

Figure 8.
Original Data Showing Polyatomic Ions Shifted to Larger Pulse Heights

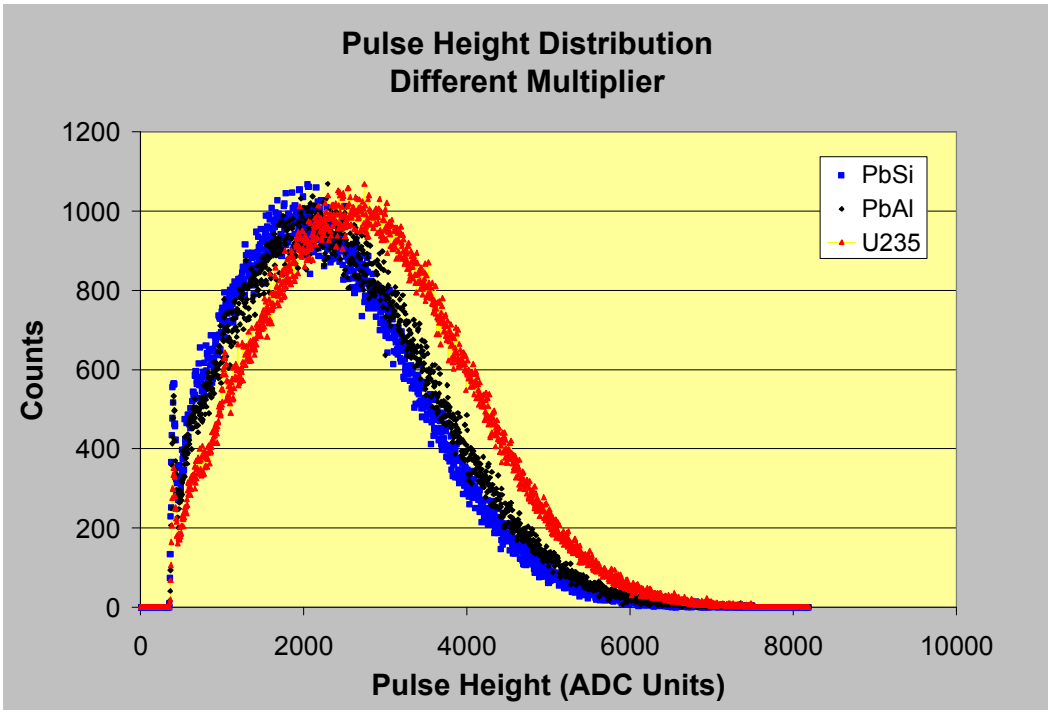

Figure 9.
Subsequent Data with Relative Positions of Atomic & Polyatomic Ions Reversed

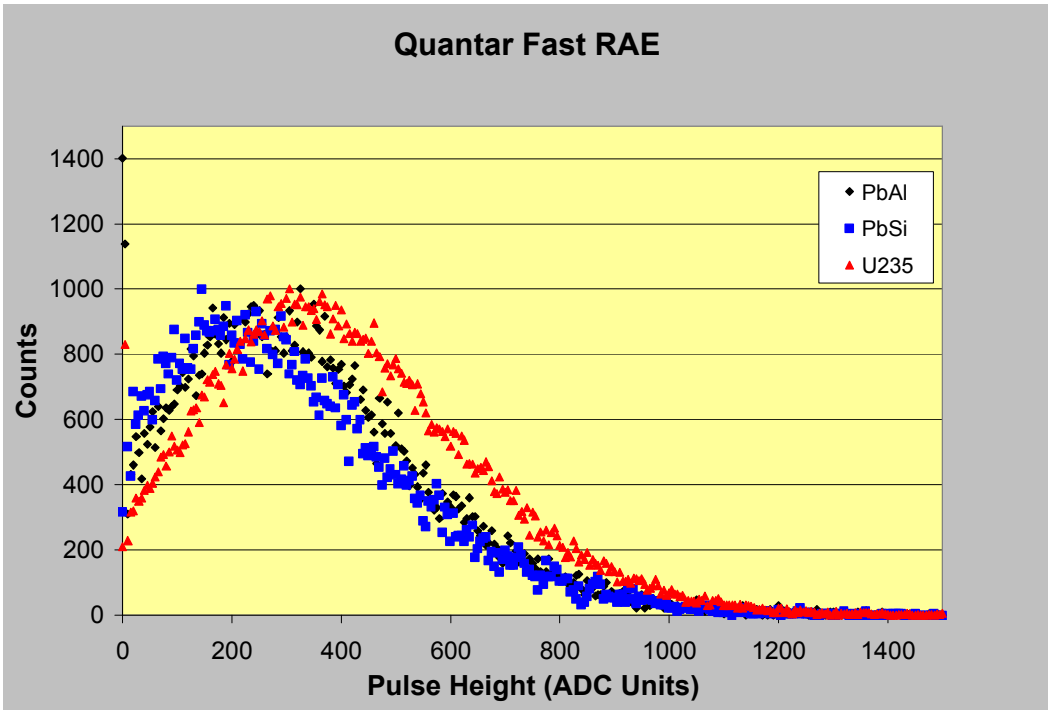

Figure 10.
Results from RAE are Similar to Current Ion Multiplier Results

Post-Accel Characterization

For the proposed rejection scheme to work, it does not matter whether the polyatomic distributions are shifted to smaller or larger pulse heights than the atomic distributions. However, it is important that these distributions remain separated in a reproducible way. Therefore, it was necessary to explore the cause of the differences between the initial set of experiments and subsequent sets of experiments. We first sought to determine the effect of ion impact energy on the atomic and polyatomic PHD using the post-acceleration option on the NIST ims-4f.

As one can see in Figure 11, as the post-acceleration voltage is increased (ion impact energy is increased), the PHD shift towards increased pulse heights. In fact, the primary purpose of post-acceleration is to increase the number of pulses due to incoming ions that exceed the threshold of the discriminator in the ion counting circuitry without a concomitant increase in the number of noise pulses that exceed the same threshold. This effect leads to an increase in detection efficiency (number of ions counted/number of ions incident on the detector) and, therefore, sensitivity in the measurement. This can be seen in Figure 12, in which we change the post-acceleration potential while maintaining a stable ion beam of $^{235}U^{+}$. This graph is the result of single point measurements at every post-acceleration potential, but the general trends were verified several times using both $^{235}U^{+}$ and other species. Most importantly, there is a 21% increase in the measured count rate at a post-acceleration voltage of 10 kV over that at 0 kV. We also noticed that the count rate decreases markedly as the ion energy is decreased from the normal 4.5 keV, which is not surprising.

However, there are two reproducible artifacts. First, the count rate increases when changing the actual post-acceleration potential from 0 kV to +1 kV (reducing the ion energy to 3.5 keV). Second, the count rate increases when changing the post-acceleration potential from +4.0 keV to +4.5 keV (reducing the ion energy from 500 eV to 0 eV). I believe that these artifacts are caused by the increased collection of secondary electrons from stray ion beams. In the case of the +4.5 keV potential, for example, the incoming ion beam is probably deflected away from the detector assembly towards some other surface where it can release secondary electrons upon impact. Unfortunately, this artifact inhibits the ability to measure the behavior of low-energy species, similar to those that are formed upon fragmentation of polyatomic ions upon impact with the multiplier cathode.

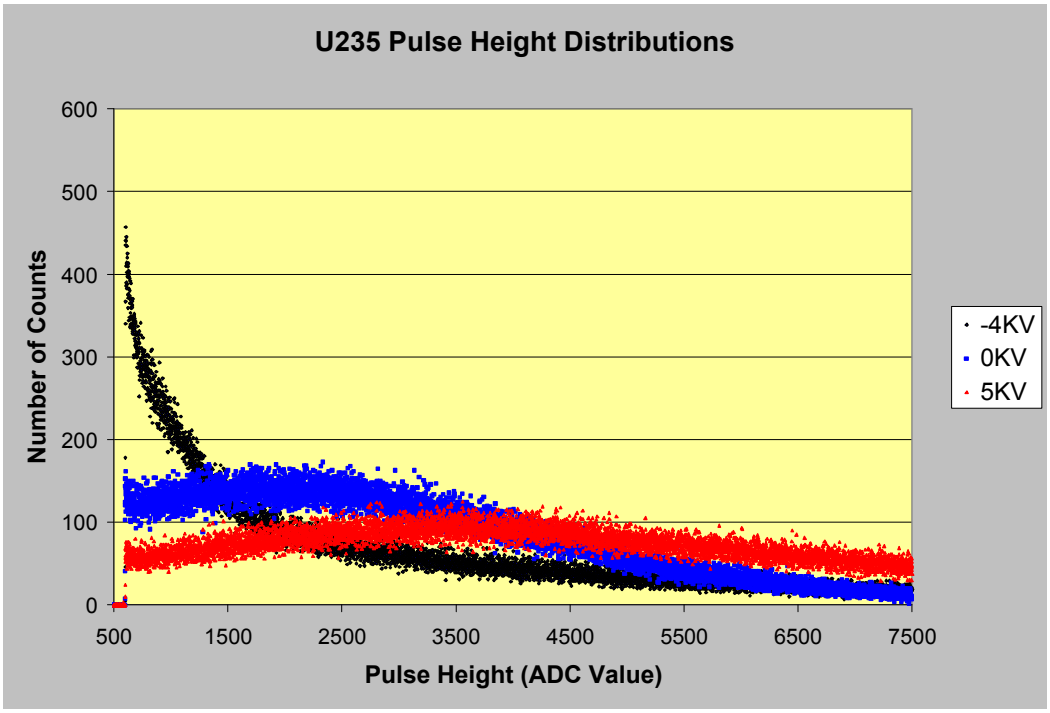

Figure 11.
Variation in Pulse Height Distributions with Post-Acceleration Voltage

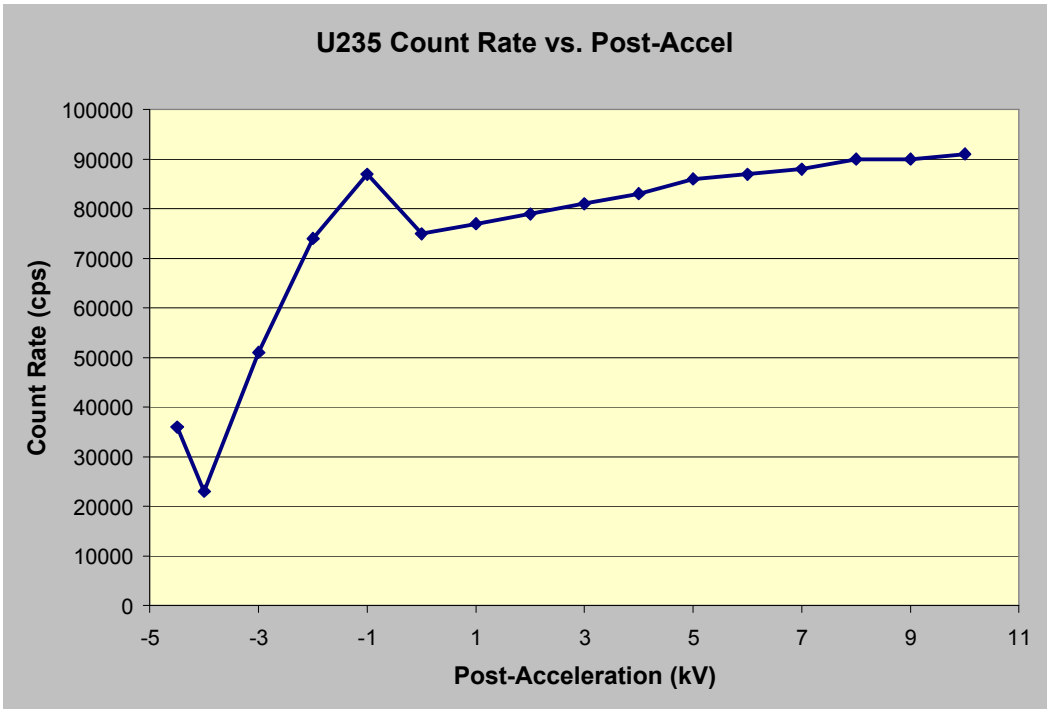

Figure 12.
Variation in Count Rate versus Post-Acceleration Voltage

In Figure 11, we also see that the pulse height distributions broaden substantially with increasing post-acceleration voltage. According the analysis of Slodzian et al.[20], the width of

[20] G. Slodzian, M. Chaintreau, R. Dennebouy, and A. Rousse, Eur. Phys. J. AP, 14, 199-231 (2001).

the pulse height distribution, expressed as the FWHM, (L in the nomenclature of the paper), increases with N_p or the average number of electrons per incoming ion released at the first dynode. Increasing post-acceleration has the effect of increasing N_p. Since we did not change the multiplier voltage during these experiments, N_e, or the average number of secondary electrons released at subsequent dynodes per incoming primary electron, should remain relatively constant.

The general behavior of the PHD versus post-acceleration voltage is shown in Figure 13. As the post-acceleration voltage is increased, the PHD shifts toward larger pulse heights (increasing γ or N_P), reaches a maximum, and then shifts back towards lower pulse heights (decreasing γ or N_P). Before the PHD shifts to this maximum, the gamma values appear to increase linearly with increasing ion velocity for a given ion, as described in the literature. The Voigt centers of the pulse height distributions for different species reach their maxima at different accelerating voltages. The Voigt widths and the gamma values also follow a similar pattern.

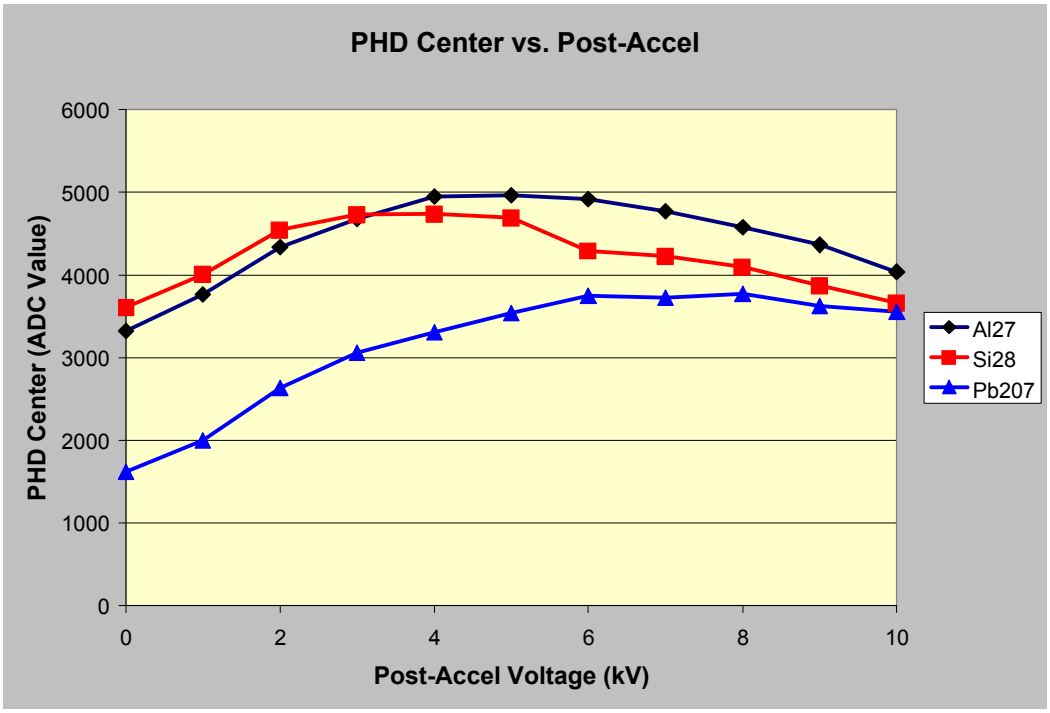

Figure 13
Shift in Pulse Height Distributions with Post-Acceleration Voltage

This behavior was unexpected. Several examples of this sort of behavior are reported by Kaminsky,[21] but the maxima occur at much higher impact energies, e.g. 500 keV for He^+ impact on Mo.

[21] M. Kaminsky, Atomic and Ionic Impact Phenomena on Metal Surfaces (New York: Springer-Verlag, 1965), pp. 300-339..

ETP Cathode & Dynode

In an attempt to understand this behavior, I investigated the structure of the ETP multiplier dynodes. I sacrificed the conversion dynode (first surface of the multiplier) and the first anode of 3 different ETP Model AF133 multipliers for analysis by X-ray fluorescence (XRF) and X-ray photoelectron spectroscopy (XPS). The first ion multiplier that we used (No. 9378) gave results in accord with the theory for metals and had good and stable gain. The subsequent multipliers that we used gave results in accord with the theory for oxides and had poor gain upon installation that degraded rapidly.

XRF analysis, which can sample to a depth of hundreds of μm, showed that the base material of the ETP dynodes was stainless steel. XPS is more surface sensitive and samples the top 100 Å or so of the material. Figure 14 shows a representative XPS spectrum of the dynode material. The surface is predominately Al_2O_3, but with F, Cu, S, Cl, and N. Carbon is commonly found in XPS spectra due to surficial contamination.

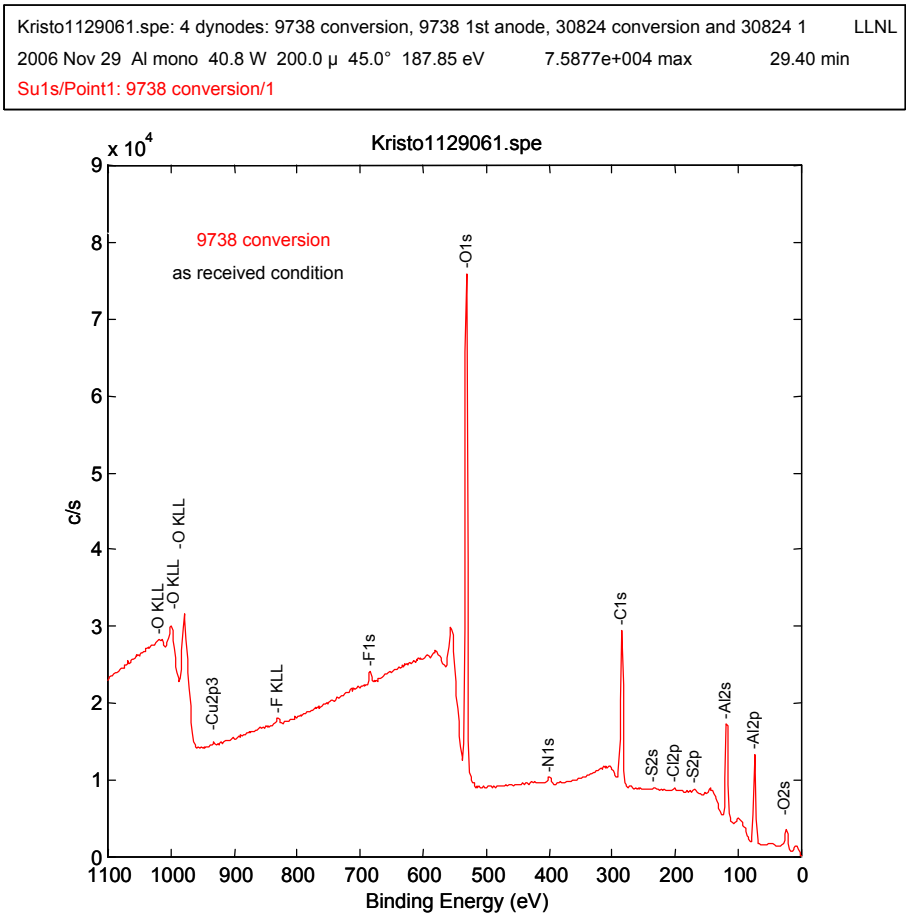

Figure 14
XPS Spectrum from Cathode of Multiplier 9738.

Figure 15 shows a representative XPS depth profile. In a depth profile, an auxiliary Ar^+ beam is used to sputter into the material, while XPS spectra are taking at various depths. The intensity of various species are then plotted as a function of sputtering time or depth (through

knowledge of the sputter rate). From these depth profiles, we determined that the stainless steel is covered by a thick (>1000 Å) layer of Al. The outermost layers of the cathodes and dynodes, though, are Al_2O_3. XPS spectra of the Al layer (beyond the Al_2O_3 surface) detected only Al and O and none of the other trace elements (F, Cu, S, Cl, and N) detected at the surface of the dynodes.

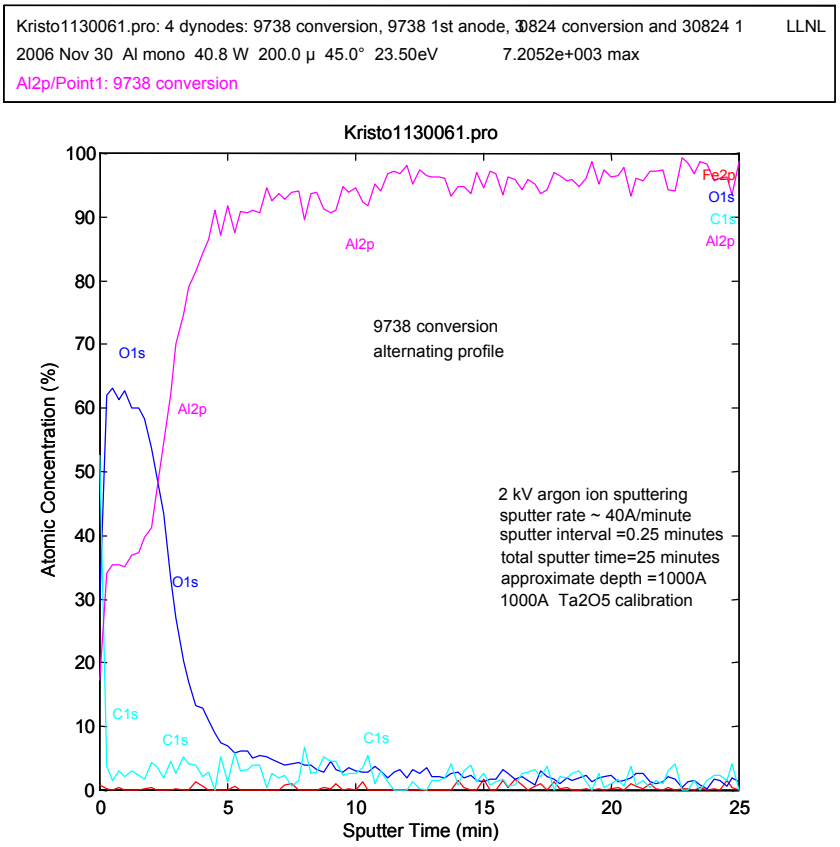

Figure 15
XPS Depth Profile of the Cathode of Multiplier 9738.

From the depth profiles, I calculated the thickness of the Al_2O_3 layer as the point at which the oxygen signal had decayed to 50% of its maximum value. The sputter time was converted to depth by using the a sputter rate of 28.2 Å/minute calibrated against an Al_2O_3 thickness standard. The resulting depth measurements are reported in Table 3.

Table 3.
Thickness of Dynode Oxide Layer

Serial No.	Useful Life (months)	Higher PHD	Conv. Dyn. Oxide	Anode Oxide
5323	9	NA	120 Å	102 Å
9378	45	Polyatomic	78 Å	94 Å
30824	12	Atomic	89 Å	136 Å

The data in Table 3 suggest that better performing (more stable gain, longer useful life) multipliers like No. 9378 have thinner Al_2O_3 layers than poorer performing multipliers like Nos. 5323 or 30824. Of course, more multipliers would have to be sacrificed and analyses performed to confirm this. However, as the thickness of the Al_2O_3 layer increases, one would

expect the surface to perform more like an Al_2O_3 surface and less like a metal surface. Multiplier No. 9378 provided the results shown in Figure 8, which are in accord with the theory for metals, while multiplier No. 30824 provided the results shown in Figure 9, which are in accord with the theory for Al_2O_3.

Microchannel plates, which accomplish the ion-electron conversion and electron amplification in an RAE, are plated with Inconel.[22,23] However, the ions that are detected typically impact the detector in the microchannels, rather than on the metal surface. The channels are formed in a heavily lead-doped glass, so it may be reasonable to expect that RAE pulse heights will behave more like an oxide surface than a metal surface, as confirmed by the results shown in Figure 10.

Ion Simulations

The escape depth of secondary electrons depends both on the material and the electrons' energy, but is estimated to be between 10 and 25 Å. I used the SRIM program to model the implantation behavior of ions at impact energies from 4.5 keV (no post-accel) to 14.5 keV (10 keV post-accel).[24] As shown in Figures 16-18, the mean implantation depth of Al^+ into Al_2O_3 increases from 56 to 148 Å as the Al^+ energy increases from 4.5 keV to 14.5 keV. Over the same energy range, the mean implantation depth of $^{235}U^+$ increases from 50 Å to 86 Å. For every material, there will be two competing effects. The first effect will be a general increase in the number of electrons released with increasing impact energy. The second will be an increase in the percentage of electrons released at depth greater than their escape depth. These two effects should lead to a maximum in the average pulse height (measured as gamma or the Voigt center) at some impact energy, although reports in the literature suggest that this energy may be larger than energies used in these experiments.

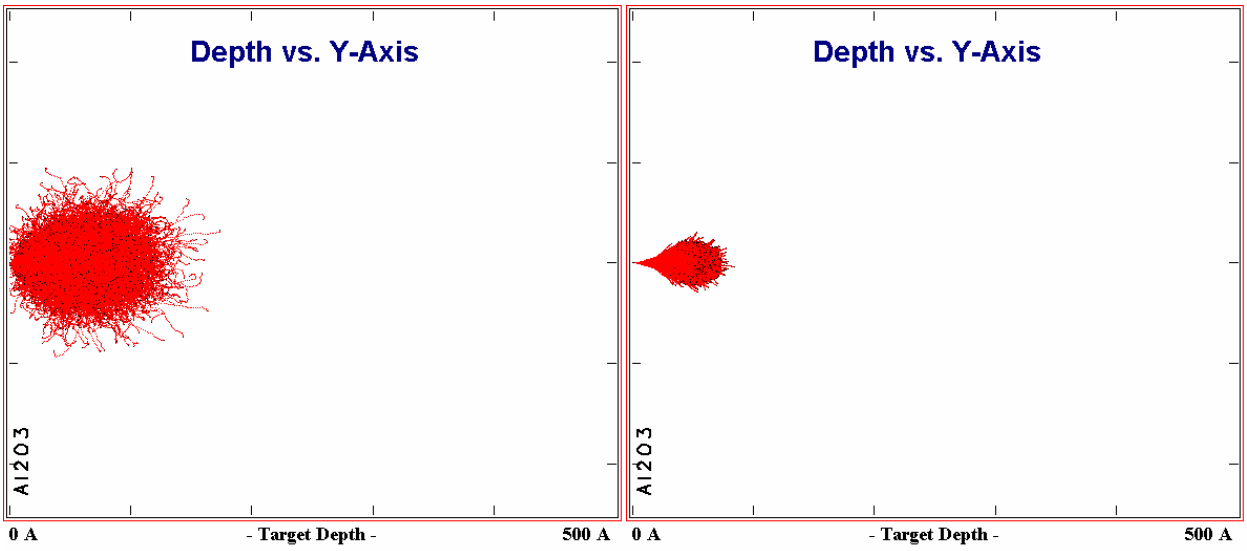

Figure 16
SRIM Simulation of 4.5 keV Al^+ (left) and U^+ (right) into Al_2O_3

[22] S. H. Siddiqui, J. Appl. Physics 48 (1977) 3053.
[23] J. L. Wiza, Nucl. Instrum. Methods 162 (1979) 587.
[24] SRIM Program, IBM Corporation.

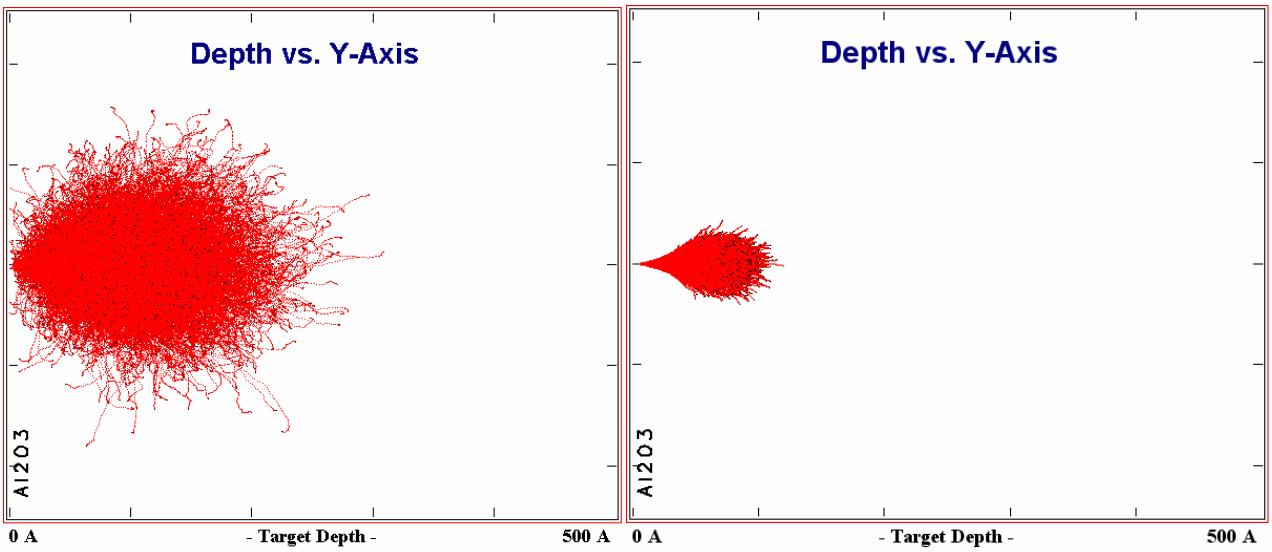

Figure 17
SRIM Simulation of 9.5 keV Al^+ (left) and U^+ (right) into Al_2O_3

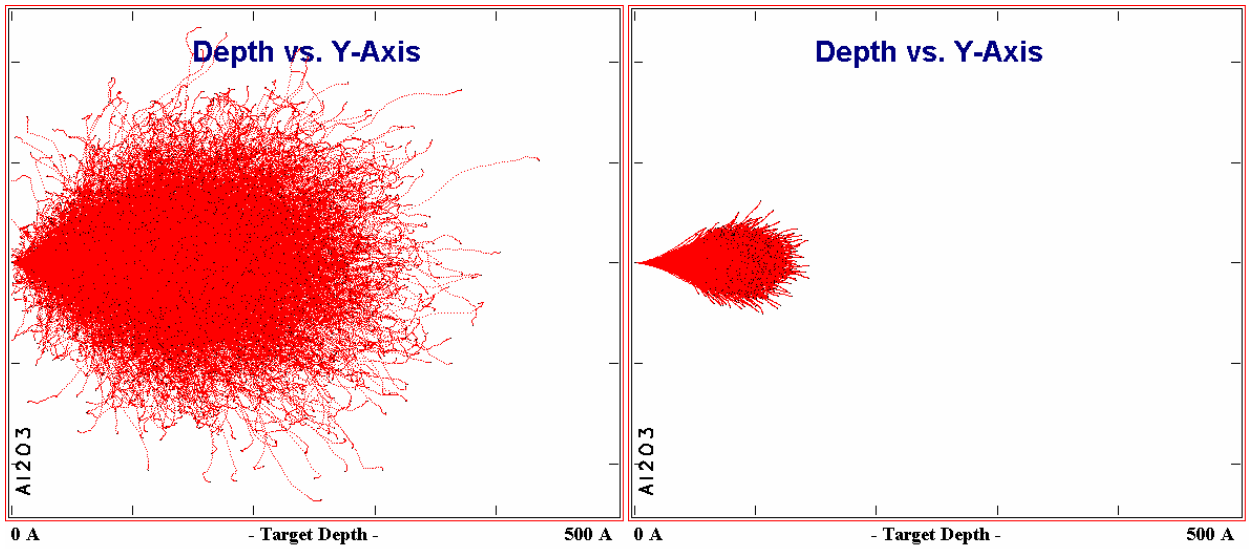

Figure 18
SRIM Simulation of 14.5 keV Al^+ (left) and U^+ (right) into Al_2O_3

For the particular situation of the ETP multiplier, though, increased ion impact energy will increase sampling of the Al layer, which has metal ion-electron emission behavior, and decrease sampling of the Al_2O_3 layer, which has oxide ion-electron emission behavior. Thus, the nature of the "polyatomic vs. atomic" effect should change with impact energy.

Furthermore, Al_2O_3 is believed to have greater secondary electron yield than Al. Certainly, the secondary electron yield for Al_2O_3 is 28% higher than Al for electron stimulated emission.[25] It

[25] B. N. Laprade, R. Prunier, R. Farr, and R. Leclerq, Poster 1340-17P, presented at the 2005 Pittsburgh Conference.

may be the increased sampling of Al with its lower secondary ion yield that leads to a maximum in the position of the PHD at energies in the mid-keV range.

The Effect of Post-Acceleration on Ions at M/Z 235

Figures 19 and 20 show how the pulse height distributions shift with post-accelerating voltage for $^{235}U^{+}$, $^{207}Pb^{28}Si^{+}$, and $^{208}Pb^{27}Al^{+}$. The data are the mean, plus or minus one standard deviation, from 3 replicate measurements of the pulse height distributions. These figures do not include the data at reduced ion energies, since those data appear to be affected by collection of secondary ion electrons and since the peak-fitting of the resulting pulse height distributions to a Voigt function is unreliable. The ETP electron multiplier on the NIST instrument gives a $^{235}U^{+}$ pulse height distribution shifted to larger pulse heights than the PbSi and PbAl species – similar to all but the first experiments at LLNL. However, as the ion impact energy is increased, the difference between the atomic and polyatomic distributions decreases and, as measured by the center of the distribution (Figure 20), becomes statistically the same at 9-10 keV. The gamma measurements (Figure 19) also become closer together as the ion energy increases, although the gamma for $^{235}U^{+}$ is still noticeably higher than the polyatomic species even at 10 keV. In either case, though, the polyatomic distributions never appear at noticeably larger pulse heights than the atomic distribution at any post-accelerating voltage and it is not clear that they might do so at potentials higher than 10keV either.

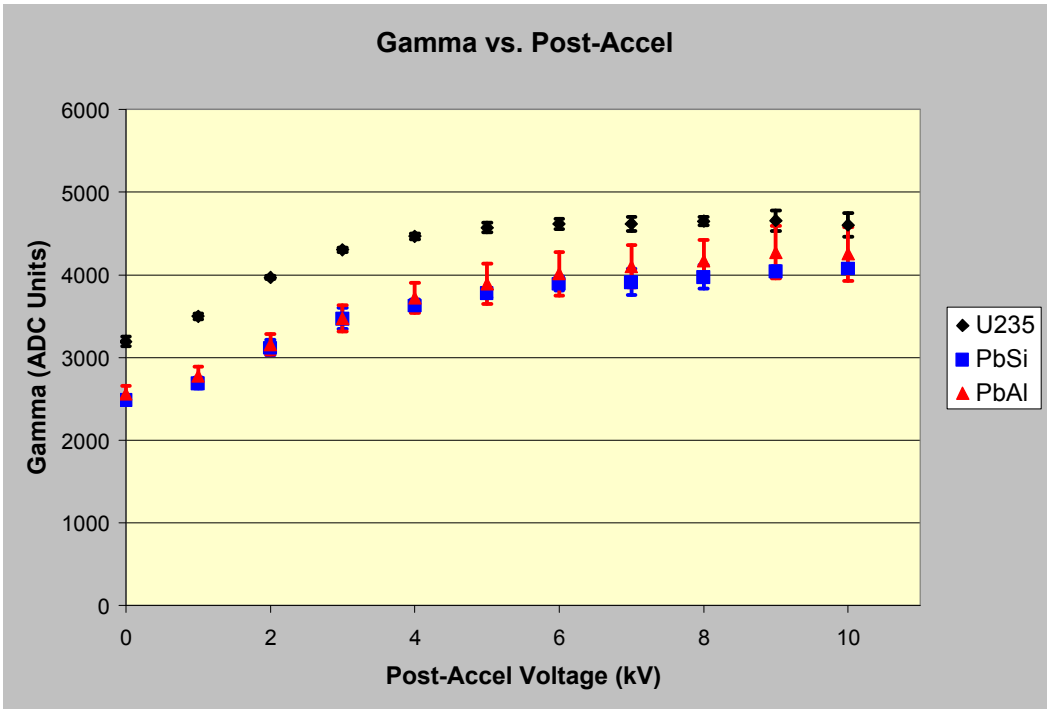

Figure 19.
Variation in Gamma versus Post-Acceleration Voltage for Species at M/Z=235

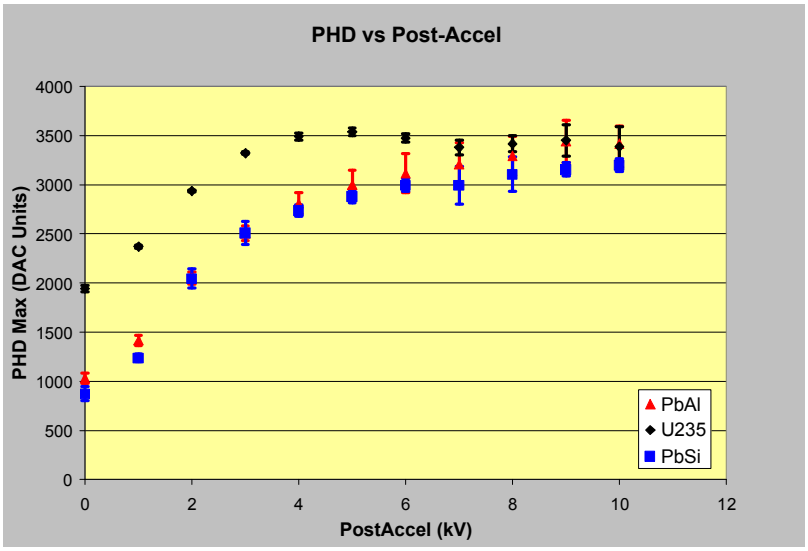

Figure 20.
Variation in Center of PHD versus Post-Acceleration Voltage for Species of M/Z-235

This behavior probably represents the effect of increased sampling of the underlying Al layer. This layer behaves in accordance with the theory for metals (polyatomic PHD shifted to larger pulse heights than atomic PHD), yet has decreased secondary electron emission relative to Al_2O_3. This is complicated behavior, but it is clear that increased ion energy does not lead to a complete reversal of behavior from oxide-type to metal-type, i.e., it affects the magnitude of the effect, but not the type of the effect.

Discussion

There are several unique aspects of this work compared to other work reported in the literature. First, we are looking at species of much higher mass than those considered in the early papers that examined the differences in pulse height distributions between polyatomic and atomic ions of the same mass, although not as high as some of the more recent papers that investigated the impact behavior of cluster ions ($(H_2O)_n^+$ or V_n^+). In addition, one of the atoms in the diatomic ions that we studied (Al in PbAl, Si in PbSi) carries a very small fraction of the original ion energy of the incoming polyatomic ion (~ 700 eV for a 4.5 keV incoming ion) upon disassociation. Consequently, the number of secondary electrons emitted by the smaller nucleon, or, in fact, whether it emits any secondary electrons at all, may be extremely dependent on the state of the conversion dynode surface.

However, it appears that the differences in behavior seen between the earlier results with multiplier No. 9738 and the later results with multiplier No. 30824 are more related to the thickness of the Al_2O_3 layer on the cathode. I made several different measurements of the "polyatomic vs. atomic" effect over the lifetime of No. 30824 and they all showed similar behavior. Therefore, although the behavior might vary from multiplier to multiplier based upon the thickness of the Al_2O_3 coating, it appears that the behavior will be stable and reproducible for each multiplier over its lifetime. If the electron multiplier has a thinner Al_2O_3 coating, then it will behave more like a metal and the polyatomic PHD will be shifted towards larger pulse heights than the atomic PHD. If the electron multiplier has a thicker Al_2O_3 coating, then it will

behave more like an oxide and the atomic PHD will be shifted to larger pulse heights than the polyatomic PHD.

Not all secondary electron multipliers have the Al_2O_3/Al/stainless steel layered structure of the ETP multipliers. A multiplier with metal dynodes, e. g., CuBe, would, of course, be expected to behave like a metal with the polyatomic PHD shifted towards larger pulse heights than the atomic PHD.

The RAE is the intended application for this technology. Since the RAE is made of lead-doped glass and not of a layered material, it is likely that the "polyatomic vs. atomic" behavior will be reproducible both from one set of microchannel plates to another and over the lifetime of a given set of microchannel plates. The RAE PHD's are expected to behave according to the oxide model with the atomic PHD being shifted towards larger pulse heights than the polyatomic PHD.

As mentioned previously, the pulse height information already exists in the Ultrafast RAE electronics.[26] The RAE detector provides 4 outputs from each of the 4 corners of the square resistive anode. These signals are usually designated A, B, C, and D. The X position is calculated as (A+B)/(A+B+C+D); the Y position is calculated as (B+C)/(A+B+C+D). In the electronics, the 4 primary signals are added to form 3 intermediate signals (A+B), (B+C), and (A+B+C+D). These 3 signals are converted into digital form and used to calculate X & Y. In the updated version of the Ultrafast RAE, currently being designed at LLNL, the digitized (A+B+C+D) value, along with appropriate control signals, will be made available to the PSEARCH-PXT acquisition system.

I detected no significant differences between the widths of the PHD for $^{235}U^+$, $^{207}Pb^{28}Si^+$, and $^{208}Pb^{27}Al^+$. The excellent reproducibility of the PHD widths (Table 1) suggest that the presence of significant amounts of any species whose pulse height distribution lies greater than 5% (2-σ) away from the standard $^{235}U^+$ PHD can be detected as an anomalous increase in the width of the acquired PHD. The "standard" $^{235}U^+$ PHD can be easily measured at the start of each campaign of analyses. In addition, we have had good success in deconvolving simulated PHD of $^{235}U^+$ and either $^{207}Pb^{28}Si^+$, and $^{208}Pb^{27}Al^+$. We have not yet had good success in deconvolving PHD of $^{235}U^+$ and both interferences. So, the presence of multiple interferences during an analysis may be problematic for the peak-stripping algorithm.

[26] A. Liu, B. Woo, and R.W. Odom, *Rev. Sci Instrum*. 71 (2000), 4144.